LAWRENCE
LIVERMORE
NATIONAL
LABORATORY

LLNL-PROC-595853

Correlation of UV damage threshold with post-annealing in CVD-grown SiO2 overlayers on etched fused silica substrates

M. Matthews, N. Shen, S. Elhadj, P. Miller, A. Nelson, T. Laurence, J. Hamilton

October 26, 2012

SPIE Laser Damage
Boulder, CO, United States
September 23, 2012 through September 26, 2012

Correlation of UV damage threshold with post-annealing in CVD-grown SiO_2 overlayers on etched fused silica substrates

Manyalibo J. Matthews*, Nan Shen, Selim Elhadj, Philip E. Miller, A. J. Nelson, Ted A. Laurence and Julie Hamilton, Lawrence Livermore National Laboratory, 7000 East Ave., Livermore, CA 94550

ABSTRACT

Chemical vapor deposition (CVD) has been used for the production of fused silica optics in high power laser applications. However, relatively little is known about the ultraviolet (UV) laser damage threshold of CVD films and how they relate to intrinsic defects produced during deposition. We present a study relating structural and electronic defects in CVD films to the 355 nm pulsed laser damage threshold as a function of post-deposition annealing temperature (T_{HT}). Plasma-enhanced CVD, based on SiH_4/N_2O under oxygen-rich conditions, was used to deposit 1.5, 3.1 and 6.4 μm thick films on etched SiO_2 substrates. Rapid annealing was performed using a scanned CO_2 laser beam up to T_{HT}~2100 K. The films were then characterized using X-ray photoemission spectroscopy (XPS), Fourier transform infrared spectroscopy (FTIR), and photoluminescence (PL). A gradual transition in the damage threshold of annealed films was observed at T_{HT} up to 1600 K, correlating with a decrease in NB silanol and broadband PL emission. An additional sharp transition in damage threshold also occurs at ~1850 K indicating substrate annealing. Based on our results, a mechanism for damage-related defect annealing is proposed, and the potential of using high-T_{HT} CVD SiO_2 to mitigate optical damage is also discussed.

*ibo@llnl.gov; phone 1 925 424-6762; fax 1 925 423-0792

1. INTRODUCTION

While all optical materials have intrinsic absorption properties that ultimately lead to damage at sufficiently high laser intensities, damage at fluences well below the band gap (~9 eV) have been found to limit the performance of even the highest quality optical components [1]. Macroscopic mechanical defects such as micro-fractures and scratches resulting from grinding, polishing, or handling processes have a high propensity to damage [2, 3]. Photoluminescence (PL) from electronic transitions has been observed from these structures but with much shorter life-time than the known point intrinsic defects [2]. At the same time, intrinsic point defects associated with non-bridging oxygen hole centers (NBOHC) and oxygen deficient centers (ODC) have also been associated to laser damage in silica [4] [5] [6]. In addition to these intrinsic defects, extrinsic defects in the form of impurities left by the polishing process, or introduced through environmental contamination, can also lead to absorption of laser light and damage [7]. A deeper understanding of different types of light absorbing defects in silica and methods to mitigate them could shed light on the physics of laser damage processes and facilitate development of more effective damage mitigation strategies. Indeed, localized CO_2 laser annealing of silica optics at high temperatures has been demonstrated to greatly improve laser damage thresholds [8, 9]. One approach to study intrinsic defects, which limit both bulk and surface silica optics performance, would be to obtain high purity and optical quality CVD-based SiO_2 and probe the effect of rapid, high temperature annealing on damage threshold. T date very few [10] UV laser damage threshold measurements of CVD silica films have been performed, and we are unaware of any studies in which a SiO_2 capping layer on fused silica has been demonstrated as a means of improving the damage threshold of laser optics or for mitigating defects on such optics.

In this work, we compare the microstructure and intrinsic defect populations of defect-rich SiO_2 thin films with their measured UV damage thresholds as a function of heat treatment temperature (T_{HT}) from focused CO_2 laser heating. High-purity, SiO_2 films were first deposited using plasma-enhanced (PE) CVD based on SiH_4/N_2O precursor chemistry. Subsequent laser treatments were performed using a scanned CO_2 laser beam operating at 10.6 μm wavelength such that the laser energy is efficiently coupled to silica resulting in localized heating. At a scan rate of 50 μm/s, our results indicate a sharp increase in the 355 nm, 3ns pulse laser damage threshold for laser-based annealing $1600<T_{HT}<2000$ K. Temporally-resolved PL mapping of as-deposited CVD films indicates a high concentration of electronic defects relative to the etched substrate, which are effectively annealed at high T_{HT}. Interestingly, PL lifetimes were shown to first decrease as a function of T_{HT} then increase indicating a transition in local order as interacting non-bridging structures become bridged/polymerized. The change in PL intensity versus T_{HT} roughly correlated with that of the intensity of non-bridging (NB) silanol modes as characterized by Fourier transform infrared spectroscopy (FTIR). In contrast, the average Si-O-Si bond angle derived from the IR spectra evolved monotonically up to 1600 K, and then stabilizes for T_{HT} >1600 K. These results suggest that mid-range ordering of the silica network, affecting bond angles, is first required for damage precursor healing, followed by short-range ordering which quenches defects associated with damage initiation. The potential use of rapidly annealed CVD overlayers as a means to mitigate or passivate damage on high power laser optical surfaces is also discussed.

2. EXPERIMENTAL

2.1. Sample preparation

All samples were processed at the MicroFabrication facility at LLNL and consisted of 10 mm thick, 2” round UV-grade type-III fused silica (Corning 7980). HF-etching was used to remove ~27 μm of surface material to eliminate any polishing contaminants, followed by a standard NaOH/detergent cleaning step, and deionized water rinse [11]. The samples were then piranha-etched (1:1, H_2SO_4:H_2O_4) and coated with SiO_2 using PE CVD method in a SiH_4/N_2O precursor gas at 300 mTorr with a substrate temperature of 573 K. The thickness, d, of the resulting SiO_2

films was 1.5, 3.1 and 6.4 μm. A control sample was HF etched, cleaned, and then piranha etched as described above. While clean room sample handling procedures were used throughout the cleaning and coating steps, some scratches on the uncoated side were produced from wafer carriers. Furthermore, some residue and/or haze was apparent, appearing on both coated and uncoated surfaces; coating-side residue appeared mainly underneath the coating. During characterization and damage testing regions with scratches or residue were carefully avoided

2.2. CO_2 laser treatments

Rapid thermal annealing of the silica CVD films deposited on silica was performed using localized 10.6 μm laser exposures as depicted in Fig. 1. A Gaussian $1/e^2$ beam diameter of 1 mm with powers <6 W allowed for a sufficiently large treatment areas for small-beam damage testing and material characterization with optical probes. Scanning was performed at rates between 5 and 50 μm/s by moving the sample stage, producing ~20 mm long tracks. The heat affected zone or the effective annealing zone scales with peak temperatures, beam size, and the effective beam dwell time as determined from the sample translation speed. For instance, for the maximum scan rate used, 50 μm/s, a given point on the sample surface is exposed to >90% of peak treatment temperature rise from a 1 mm beam in about 4.5 s.

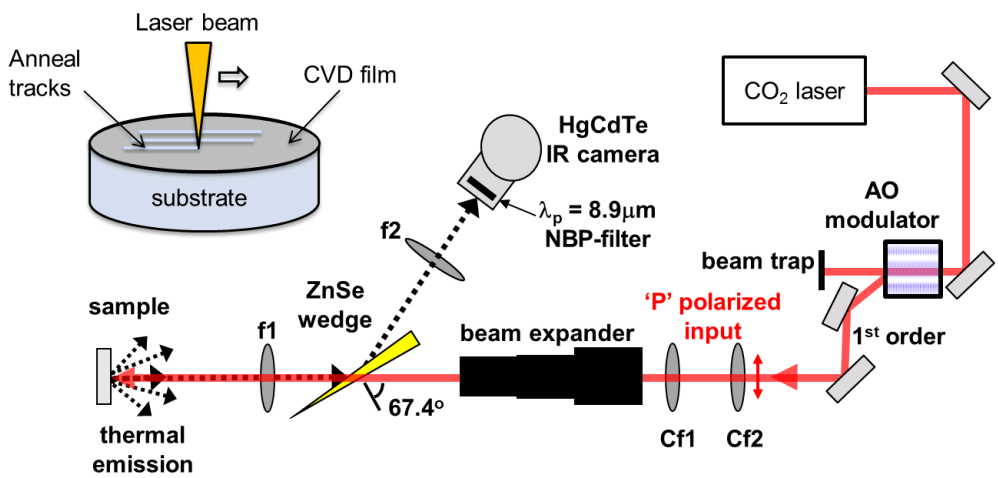

Figure 1: Experimental setup for laser heat treatment and thermal imaging of CVD films. A 10.6 μm laser beam is sent through an acousto-optic modulator and thereby attenuated to various power levels before going through beam expansion optics, a wedge and final focus lens (f1). Thermal emission is captured by f1, reflected off the wedge and sent to a calibrated HgCdTe camera bandpassed at 8.9 μm. Laser anneal tracks are created across the CVD films by scanning at various rates and at various T_{HT}.

Because the effective dwell time is long relative to the thermal diffusion time (τ_{th}~40 ms), the heating depths due to diffusion are large compared with the film thickness. Therefore, the heating across the films is assumed uniform in depth. Details of the laser used for heating and the camera and optical system used for the *in situ* measurements of the spatial profile of the temperature (T) are available elsewhere [12]. Briefly, a calibrated HgCdTe infrared camera operating at 1 Hz with a narrow bandpass cold filter (λ_c=8.9 μm) was used to capture the infrared blackbody radiation emitted from the IR-laser heated surface, which was then used to resolve the *T* profiles over time from each captured frame. The spatial resolution achieved by the IR thermal imaging system was ~40 μm. The variability in the T_{HT} profiles is mostly due to the fluctuation in the laser power of ~5%. In the results that follow, we report time-averaged (peak or local) heat treatment temperatures for t>4.5 s and up to the laser turn off time unless otherwise noted. Individual laser treatment tracks were made covering a peak temperature range of

1300~2400 K, which corresponds roughly to the range between the glass transition point and the maximum sub-evaporation temperature over the time scales considered here.

2.3. Damage testing and defect characterization

Along with damage testing, all films were characterized using FTIR, PL and XPS. Large aperture, fixed angle (~16°) incidence IR reflectance measurements of coatings prior to laser treatment and from 360 to 4000 cm^{-1} were made using a Perkin Elmer Spectrum One system with a resolution of 4 cm^{-1} and accuracy of 0.1 cm^{-1}. Spatially resolved (~10 μm spot size) normal incidence IR reflectance scans of laser-treated regions over the same spectral range were made using a coherent synchrotron radiation source (Beamline 5.4, Advanced Light Source, Lawrence Berkeley National Laboratory) coupled via 32x/0.65NA reflective optics to a Spectra Tech Nic-Plan IR microscope. The synchrotron based FTIR (SR-FTIR) measurements were accurate to 0.09 cm^{-1} with a resolution of 4 cm^{-1}. A lateral step size of 50 μm was used to measure variations in IR reflectance as a function of local thermal treatment. Additional details of the SR-FTIR system are described elsewhere [6].

The pulsed laser damage resistance of the sample was assessed using small beam R/1 laser exit surface damage testing [13]. A Coherent Infinity Q-switched Nd:YAG laser operating at 355 nm, ~3 ns was used in the test. The laser pulse energy and its spatial profile are monitored by picking off a fraction of the beam and recording it using a charge coupled device (CCD) camera. The Gaussian beam has a measured $1/e^2$ beam radius of r~40 μm which was used to determine peak axial fluence as $\phi=2E/\pi r^2$ where E is the incident pulse energy accounting for reflection loss from the sample. An imaging microscope is set up to observe the sample under laser irradiation. During damage testing, the laser pulse energy is slowly ramped up with ~5 J/cm^2 steps until damage is registered on the imaging CCD camera. Each R/1 damage threshold measurement is the average of ~10 spatially separate damage test sites. Test scans along the CO_2 laser treated tracks excluded the first ~3 mm of the tracks to allow temperature to reach steady-state. Large area damage testing was also performed and used to compliment the small beam testing in the low T_{HT} regime. Further results from large area testing will appear in a future publication.

Confocal Time-resolved Photoluminescence (CTR-PL) imaging was used to probe the light-matter interactions in the deposited SiO_2 where damage thresholds were assessed . A 3.1 eV pulsed laser (400 nm, LDH-P-C-405B, Picoquant) is focused using a high numerical aperture objective (20X, 045NA Mitutoyo objective) onto a fused silica sample. Scattering and luminescence excited by the laser are collected by the same objective and focused onto a confocal pinhole (100μm; excluding out-of-focus luminescence). One spectral channel (>440 nm) and a scattering channel are monitored by avalanche photodiodes (Micro Photon Devices PDM 50CT). Each detected photon is time-stamped with its absolute arrival time (50 ns resolution) and its arrival time relative to the laser pulse (measuring PL lifetime with 150-300 ps resolution) using a time-to-digital converter (PicoHarp 300, Picoquant). The sample is scanned in 3 dimensions using a motorized stage controlled by an ESP301 controller (Newport). Data acquisition and analysis are performed using custom software written in LabVIEW.

XPS was used to investigate the surface chemistry of as-deposited CVD film and after CO_2 laser treatment. XPS analysis was performed on a PHI Quantum 2000 system using a focused monochromatic A; $K\alpha$ x-ray (1486.7 eV) source for excitation and a spherical section analyzer. The instrument has a 16-element multichannel detection system. A 100 μm diameter x-ray beam was used for analysis. The x-ray beam is incident normal to the sample and the x-ray detector is at 45° away from the normal. The pass energy was 23.5 eV giving an energy resolution of 0.3 eV that when combined with the 0.85 eV full width at half maximum (FWHM) Al $K\alpha$ line width gives a resolvable XPS peak width of 1.2 eV FWHM. The collected data were referenced to an energy scale with binding energies for Cu $2p_{3/2}$ at 932.72 +/- 0.05 eV and Au $4f_{7/2}$ at 84.01 +/- 0.05 eV. Binding energies were also referenced to the C 1s photoelectron line arising from adventitious carbon at 284.8 eV. Low energy electrons were used for specimen neutralization. The sample was sputtered for 10 minutes at ~3 kV to remove surface contaminants before XPS data was collected from un-annealed film, and 3 locations along the track of sample M2063 treated at ~1900 K.

3. RESULTS

3.1. Fourier transform infrared spectroscopy

IR reflectance spectra were taken of the CVD coating following deposition using FTIR, and compared with 'pristine' etched-only surfaces. Figure 2(a) shows a typical far-IR spectra taken of the 1.5 μm thick film sample M2063 between 400 and 1450 cm^{-1}, where 4 of the 5 peaks can all be associated with fundamental Si-O vibrational modes of tetrahedral SiO_2: bridging O atom rocking at 440 cm^{-1}, symmetric stretching Si-O-Si at 790 cm^{-1}, and an asymmetric stretch Si-O-Si mode which shows a strong splitting into a transverse optic (TO) mode at ~1120 cm^{-1} and a longitudinal optic (LO) mode at ~1220 cm^{-1}. We refer to these modes as TO_1, TO_2, TO_3, and LO_3 modes respectively. In addition, a small peak near 900 cm^{-1} is also visible for the as-deposited film only in the far-IR spectrum (see inset of Fig. 2(a)) which could be assigned to (at least) one of three possible modes previously observed in SiH_4-based films: Si-N stretching mode from unintentional N doping [14], Si-H wagging mode [15] or a Si-O/Si-OH non-bridging stretching mode [16]. However, Si-N can be ruled out based on XPS results presented below which indicates no detectable N in the films, while the Si-H wagging mode should also produce a corresponding Si-H stretching mode at 2265 cm^{-1} which we did not observe in any of the films studied. We therefore assign this peak to the Si-O/Si-OH non-bridging stretching (NB) mode created either during synthesis and/or through post-deposition absorption of ambient water vapor[17]. Its density is estimated by normalizing the area

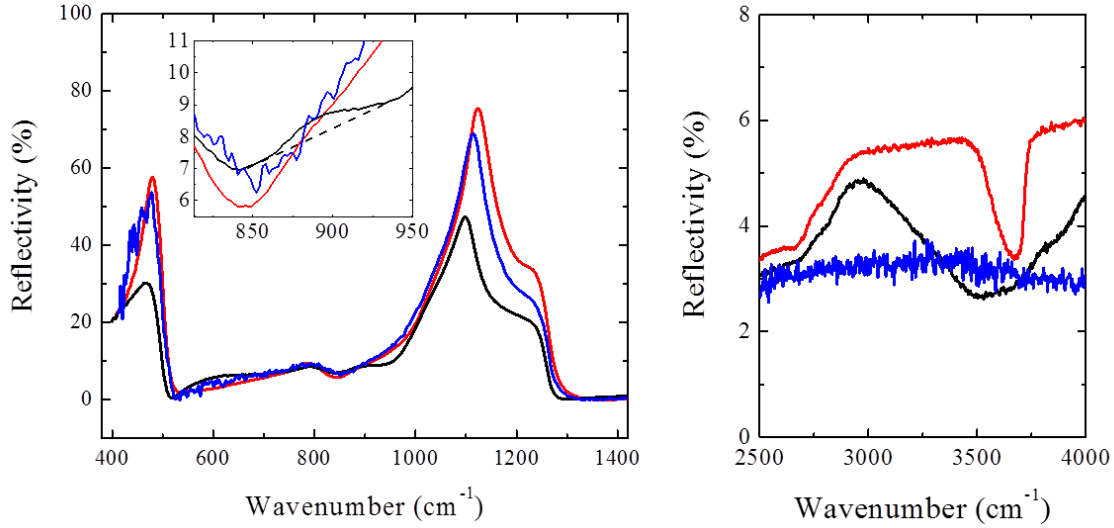

(a) (b)

Figure 2(a) and (b): FTIR spectra of as-deposited CVD film M2063 with 1.5 μm thick film (black curve), the same film treated with a 50 mm/s scanned laser beam at T_{HT}~2000 K (blue curve) and etched-only control sample (red curve). The inset of (a) shows the spectral region of the NB mode and the French curve used to approximate the peak area.

underneath the peak (Fig. 2(a) inset) to the TO_3 mode intensity. Besides the appearance of the NB mode in as-deposited films as compared with a pristine surface, the peak frequency of the TO_3 mode of the former in Fig. 1(a) shows a large red-shift of 24-30 cm^{-1} relative to that of the latter. Similarly, smaller (blue-) red-shifts of the (TO_2) TO_1 were observed and equal to (12 cm^{-1}) 16 cm^{-1}. The overall reflectivity of the as-deposited film appears lower as compared to that of the control samples, particularly in the LO-TO asymmetric stretch region (~1100 cm^{-1}). Fig. 2(b) shows the mid-IR reflectance spectra in the region of the O-H stretch vibration. For the etched-only control

samples a band near 3600 cm^{-1} corresponds to isolated, bound silanol groups (Si-OH) typical of type-III vapor-deposited glasses such as Corning 7980. However, the mid-IR spectra of the unannealed CVD sample (M2063 with 1.5 μm thick film) shows a much broader OH band, indicative of relatively high silanol concentration and interaction between OH groups which acts to soften the vibrational mode [17]. The relatively large contribution of this O-H stretch band would also tend to support the assignment of the Si-OH mode to the ~900 cm^{-1} peak. No peaks in the reflection spectra were observed in the range 1400 – 2600 cm-1. A multi-component Gaussian fit was performed on the FTIR spectra between ~840 and ~1150 cm^{-1} in order to extract the TO_3 frequency. The integrated intensity of the NB mode is estimated by drawing a baseline shown as the dashed line in Fig. 1(a), and calculating the area underneath the curve.

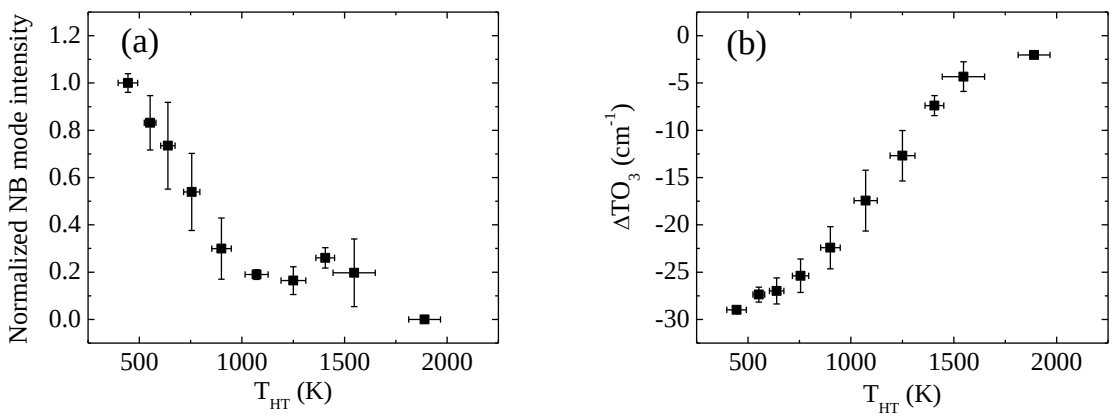

Figure 3: Evolution of the normalized intensity of the NB mode (a) and frequency of the asymmetric TO_3 mode (b) averaged across laser treatment tracks on the 3.1 μm thick film.

Following SiO_2 film deposition, the samples were locally and rapidly annealed along ~1×20 mm tracks using a focused CO_2 laser. Structural changes in the CVD films associated with the laser treatments were recorded using spatially-resolved SR-FTIR microscopy. Lateral scans across each of the laser-treated tracks resulted in spatially-dependent spectra which could be registered with thermal imaging data to yield temperature- and scan rate-dependent spectra. With increasing T_{HT} from laser heating, the polymerization of the CVD films gradually progressed, as the laser annealing indicated a decrease in NB Si-O, Si-OH in general, a blue shift of the TO_1 and TO_3 modes, and a red shift in the TO_2 mode. The total reflectivity also increased as a function of laser annealing. Because the laser treatments induce an increase in fictive temperature [18], the spectra corresponding to the most aggressive thermal treatment did not exactly coincide with that of the pristine substrate. In particular, the TO_3 mode appears at 1120-1122 cm^{-1} for the highest temperature treatments, as compared with 1123 cm^{-1} for the pristine surface indicating a slightly densified final state. The broad LO_3 mode did not appear to shift appreciably in frequency, nor change in intensity relative to the TO_3 mode which indicates that the films remained relatively smooth at the micron scale [19]. Along with changes in the longwave IR region of the fundamental SiO_2 modes, a decrease in OH peak reflectivity in the mid-IR region of film reflectivity also occurred as a function of T_{HT}. Although specific sub-features could not be discerned due to the broadness of this band, the highest temperature case (T_{HT}=2000 K) appears similar to a type-I, low OH silica with OH concentrations of less than 150 ppm by weight.

We now quantify the behavior of the CVD film in terms of frequency shift and intensities in Fig. 4 as a function of T_{HT}. We first note that the Gaussian spatial profile of the CO_2 laser beam creates a continuous varying Gaussian-like temperature profile across each treatment track. Due to the spatial proximity of laser treatment tracks (2 mm spacing between tracks), some small amount of unintentional pre- and/or post-treatment overlap potentially exists at the

boundary between tracks measured. The evolution of the TO_3 peak frequency and the NB mode intensity are plotted as a function of the measured *local* T_{HT} for two treatment tracks on the 3.1 μm thick film sample for peak treatment temperatures of 2152 K and 1950 K in Fig. 4. The monotonic shifting in the TO_3 frequency between 500 and 1500 K indicates the continuous relaxation of the glass network and approaches a maximum value that is close to pristine glass at ~1600 K. The intensity of the NB mode, on the other hand, decreases first at low T_{HT}, but increases at higher T_{HT}, peaking at ~1500 K before a drop at higher treatment temperature.

The frequency shifts of the TO_3 mode for all the laser treatment tracks on the three samples used in our study are summarized in Fig. 4 as a function of the peak T_{HT}. The dashed line is a fifth order polynomial fit to the ΔTO_3 curve shown in Fig. 3(b). The composite data is noisier as expected due to sample and local CVD deposition variability, but agrees reasonably well with the result from the single track measurement.

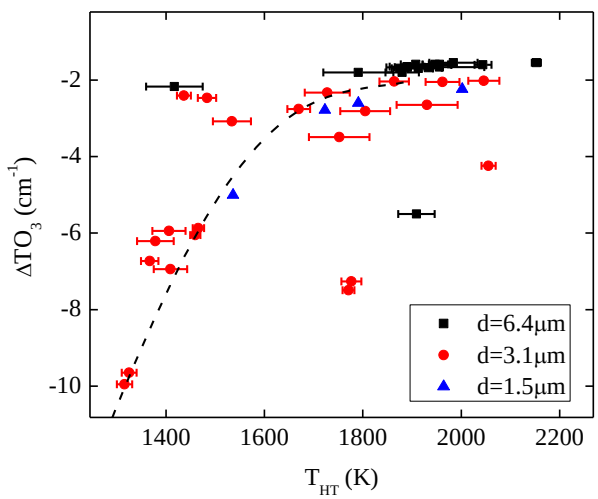

Figure 4: Frequency shift of the TO_3 mode for all treatment tracks on three samples as a function of peak T_{HT} averaged along the tracks. The dashed line is an overlay of the local TO_3 frequency data from Fig. 4(a) at T_{HT} =2152 K.

3.2. Photoluminescence mapping

The presence of a NB mode in the FTIR reflectance spectra suggested there may be a population of optically-active NBOHCs - in addition to other defects - in the CVD films that have previously been associated with optical damage [6, 20]. In order to observe more directly the electronic transitions that may be associated with these defect vibrational states, we performed confocal PL microscopy with near-UV (400 nm) laser excitation, and a 430 nm long pass filter at the collection side. Figure 5 shows a mosaic of microscopy scans (50 μm step size) taken of the 1.5 mm thick film treated at various T_{HT} and scan rates. In terms of the total defect concentration – and inferred broadband PL intensity – one would expect a gradual decrease as the films transition to a higher damage threshold state. Interestingly, the total PL signal first increased, then decreased with T_{HT}. This is in contrast to the monotonic increase in TO_3 frequency revealed by SR-FTIR but somewhat correlated with the NB oxygen mode intensity. This effect is more clearly seen in the expanded view of Fig. 6 where the PL intensity across the laser treatment tracks shows a higher PL signal at the center of the tracks as low T_{HT} but is lower for higher T_{HT}. Furthermore, by temporally-resolving the PL decay, a mean excited state lifetime of ~3.2 ns was found which followed an inverse trend with T_{HT} as compared with PL intensity. This suggests that the increase in emission was likely due to lifetime effects rather than from an increase in defect populations.

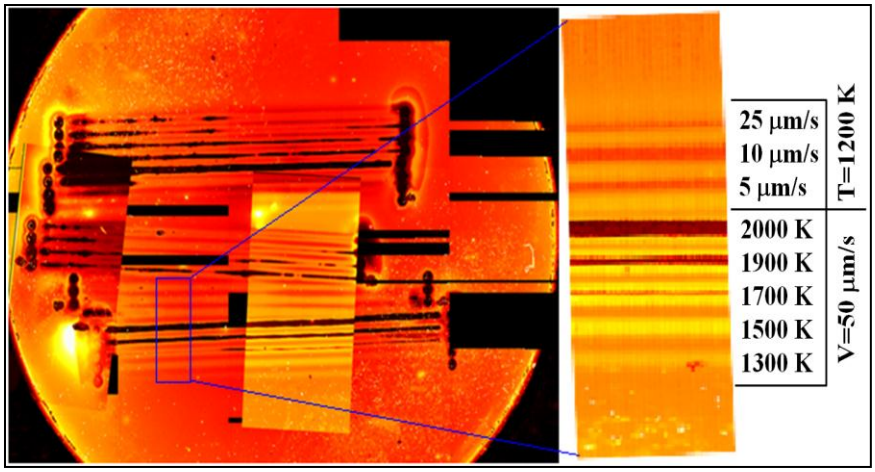

Figure 5: (a) Photoluminescence intensity mosaic of 1.5 μm thick film treated with various CO_2 laser treatments. Treatment tracks are oriented horizontally with circular fiducial marks at either end of the tracks. As shown in the expanded view of several tracks on the right side of the figure, an increase in intensity occurs as a function of T_{HT} followed by a decrease at higher T_{HT}.

3.3. R/1 laser damage test

Pre-annealed CVD films were damage tested resulting in damage thresholds in J/cm^2 of 15.0 ± 1.5 (1.5μm), 22.7 ± 2.0 (3.1μm), 19.9 ± 1.7 (6.4μm) and 45.3 ± 3.7 (control). Samples were then treated with varying CO_2 laser power (i.e. temperature) from ~3 to 6W and scan rate (i.e. dwell time) and retested. Figure 6(a) shows the normalized R/1 damage threshold as a function of the peak T_{HT} at the center of the tracks with a scan rate of 50 μm/s. For T_{HT}<1500

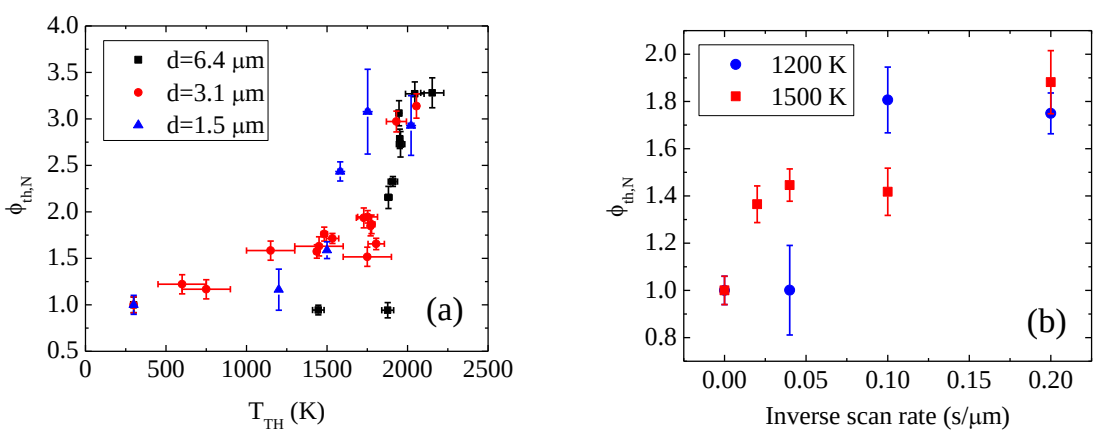

Figure 6: Normalized R/1 damage threshold measurements of the test samples as a function of T_{HT} (a) and as a function of scan rate at 1200 and 1500 K (b).

K, the damage threshold did not appear to change significantly. However, a very sharp transition in damage threshold is observed in the range 1500<T_{HT}<1700 K for the 1.5 and 3.1 μm thick films. Specifically the normalized damage threshold improves by roughly a factor of two whichcorresponds to changes from the as-deposited threshold of ~17 J/cm^2 to ~40 J/cm^2, which is close to the value of the underlying substrate. Above ~1750 K all three samples show a transition where the normalized damage threshold increases by an additional factor of 1.6 to ~65 J/cm^2, well in excess of the damage threshold of the underlying substrates. We examined two T_{HT} points – 1200 and 1500 K – for the 1.5 μm film that are near- or sub-threshold along the S-curve in Fig. 6(a) and observe the R/1 behavior as a

function of slower scan rates. The results are shown in Fig. 6(b), cast in terms of inverse scan rate where scan rates ranged from 5 to 50 μm/s. The R/1 damage threshold at zero inverse scan rate (infinite scan rate) is taken as the untreated threshold value (~17 J/cm^2). At T_{HT}=1200 K, which is just below the glass transition temperature (T_g) for type III silica (~1300 K), an increase in damage threshold is observed below a scan rate of 10~25 μm/s (effective dwell time of ~1-2.3 s), although the threshold increase apparently plateaus at ~30 J/cm^2. A similar increase is observed at T_{HT}=1500 K, with a higher threshold scan rate of >50 μm/s, and an additional increase in going from 10 to 5 μm/s.

3.4. X-ray photoemission spectroscopy

XPS was used to assess the stoichiometry, verify the purity and probe the Si and O electronic states of the films which are in general sensitive to local electronic environments. For both treated and untreated films the O/Si ratio was found to be 2.06. No residual nitrogen from the N_2O precursor gas was detected in the CVD film (detection sensitivity 10^{19} atoms/cm^3). Minimal carbon contamination was only detected on the untreated CVD film and was most likely due to organic contaminants from the environment, adsorbed into the porous structure of the film. Figure 7 compares the Si $2p_{3/2,1/2}$ spectra of the as deposited PVCVD and the laser treated track of the 6.1 μm thick sample. A single peak near 104 eV was observed corresponding to the Si^{4+} oxidation state associated with SiO_2 [21]. The Si $2p_{3/2,1/2}$ spin-orbit components were deconvolved and are centered at 103.3 and 104.0 eV for the as-deposited films. A small shift in the Si $2p_{3/2,1/2}$ spin-orbit components was observed for the laser treated area to 103.5 eV and 104.2 eV typical for pure SiO_2 (NIST XPS database), FWHM remaining the same. Correlating this chemical shift with the compositional analysis indicates that the laser treated areas have a composition and structure closer to that of bulk SiO_2 than the untreated film, consistent with the improved damage thresholds.

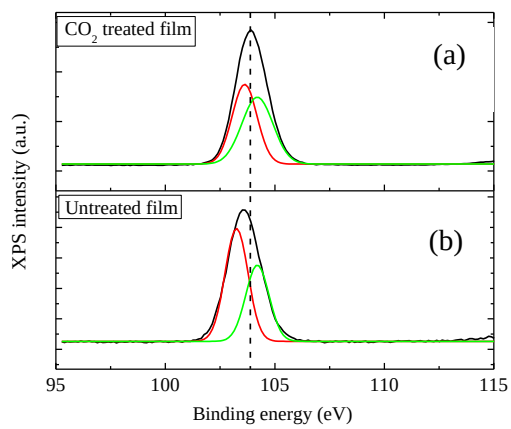

Figure 7: Si 2p binding energy of (a) laser-treated region corresponding to a peak temperature of 1900 K and (b) as-deposited CVD film measured by XPS.

4. DISCUSSION

The presence of both extrinsic (i.e. contaminants) and intrinsic defects in the silica films can lead to absorption and subsequent damage initiation under UV illumination as compared with pristine, etched silica substrates. Furthermore, if the CVD films contain nano-fractures undetectable to our instruments, the decrease in mechanical strength of the film could also lead or add to a reduction in damage threshold. Since the purity of the films in our study was reasonably high, and the damage threshold increases upon CO_2 laser heating, this suggests that the extrinsic defects are not the dominant damage precursors in the CVD films. The intrinsic defect concentration,

however, was relatively high for the as-deposited films, as indicated by both PL and FTIR measurements. The change in defect-related spectra also correlates well with the change in damage threshold of the film as it was annealed with the CO_2 laser. This suggests that intrinsic defects are the main contributors to light absorption and thus laser damage.

Shifts in the peak positions of the infrared reflectivity spectra can be related to physical modification in the internal structure of the glass network. Such changes would include a reduction in the fraction of 3- and 4-member Si-O rings, relaxation in the average Si-O-Si bond-angle and local changes in the density of the films. For example, as-deposited vapor-based silica films are expected to have densities lower than that of annealed films due to a high porosity driven by the presence of large voids and accompanying defects. The average Si-O-Si bond angle can be estimated using the central force network model [22],

$$\omega^2 = \frac{k}{m_o}(1 - cos\theta) + \frac{4}{3}\frac{k}{m_{si}}$$

where ω is the angular frequency of the TO_3 mode, k is the Si-O stretching force constant, θ is the average Si-O-Si bridging angle, and m_o and m_{si} are the mass of the oxygen and silicon atoms. With increasing laser-heat-treatment and increasing polymerization of the films, the bond-angle relaxes, and the density increases through the annihilation of NB oxygen structural defects, producing a rise in damage threshold (Fig. 6). As a prelude to this damage threshold increase, however, an increase in IR reflectivity due to NB modes is observed. An increase in IR activity of this band would be consistent with an increase in the more dipolar O- over OH structures as water and hydrogen are driven out during annealing, leading the way for bond-bridging. An increase in dipole strength due to a dangling oxygen bond could also bring about a more intense ODC PL emission through a decrease in PL lifetime.

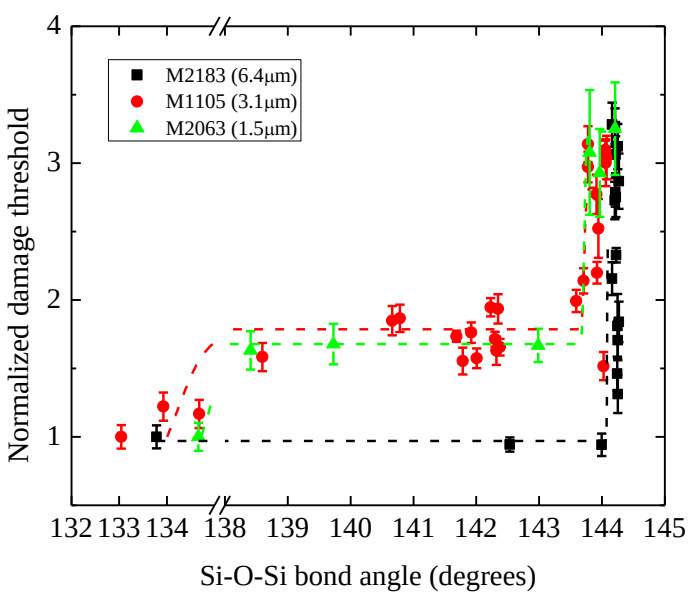

Figure 8: R/1 damage threshold measurements of three test samples as a function of the estimated Si-O-Si bond angles. Dashed lines are guides to the eye.

In our CVD samples, we have observed the vibration from the NB mode in the FTIR measurements in the un-treated film compared to the bulk SiO_2. With increasing CO_2 laser treatment temperature, the intensity of this vibration peak can be reduced to a level similar to that of pristine SiO_2. While not resolved spectrally in this study, it is presumed

that the broadband emission under 400 nm excitation would include contributions from both ODC-II and NBOHC defects [4]. The band near 3600 cm^{-1} in the FTIR data (Fig. 2(b)) also indicates that the silanol concentration in the CVD film was initally high, and decreased significantly after CO_2 laser annealing. Based on these observations, it appears that the vibration from NB oxygen in as-deposit CVD film is mainly due to the Si-OH population. As the film undergoes heat treatment, silanol is driven out through OH diffusion at lower temperatures [23]. This would explain the decrease in the NB mode intensity observed in the FTIR (Fig. 3(a)) spectra. It is important to point out that this decrease was not monotonic with T_{HT} as the shift in the TO_3 mode is shown Figs. 3(b) and 4. There was a recovery in NB vibration for T_{HT}>1000 K which peaks around ~1600 K (Fig. 4(a)), with the effect more moderate for the thinner film (3.1 μm). This increase may be the result of the interaction between molecular water and silica [17]. The fact that the PL intensity increases (and the PL lifetimes decreases) at the wings of CO_2 laser tracks with a peak around T_{HT}=1600 K supports this interpretation. Ultimately, at high enough T_{HT}, the NB mode, as well as PL, decreases again for CO_2 treated CVD films.

The onset of the damage threshold change depends strongly on the thickness of the film, with the thickest sample (6.4 μm) only showing a damage threshold increase at ~1900 K, where the underlying substrate also is annealed (Fig. 6(a)). One possibility for the disparity could be the differences in the thermal profiles through the films. Indeed, the absorption length at 10.6 μm in silica at ~1500 K is about 5.9 μm, implying that heating may not penetrate to the bottom of the 6.4 μm film. However, since thermal diffusion times are long compared to effective dwell times and the beam radius a is large compared to the absorption length, we can treat the laser beam as a CW surface source and estimate the temperature change ΔT as a function of depth z as [24]:

$$\frac{\Delta T(z)}{\Delta T(0)} = erfc\left(\frac{z}{a}\right)\exp\left(\frac{z^2}{a^2}\right)$$

The above expression yields ΔT(6.4 μm)/ ΔT(0)~0.98 or about a 30 K decrease from a surface temperature of 2000 K, far less than the differences observed in the damage threshold data between films. Since the temperature across the film depth was relatively constant for all films, this thickness-related effect on annealing may be attributed to the fact that thicker films contain significantly more defects (for a given density of defects) and therefore require more heating to overcome the population barrier before damage threshold improvement can be observed (i.e. a 'critical mass' effect). For thinner films (1.5 μm and 3.1 μm), on the other hand, the damage threshold first increased gradually to ~40 J/cm^2 at around T_{HT}=1600 K, similar to the etched silica substrate. The damage threshold improvement is accompanied by a drop in the NB mode intensity. This suggests that in CVD SiO_2 film, the population of the ODC type of defects is the main absorber of UV light and may lead to optical damage. However, we note that while the sampling depth of the TO_3 mode is less than 1 μm due to high absorptivity at ~1120 cm^{-1}, light reflected at ~950 or ~3600 cm^{-1} can probe depths that can include the substrate as well as the film, which may affect the observed intensity changes in these bands. At higher T_{HT} (~1850 K), all film sample damage thresholds improve sharply to ~65 J/cm^2. The fact that this latter increase above the ~40 J/cm^2 threshold of the substrate does not vary with film thickness implies a modification of the substrate itself. Moreover, because of the distinctly different T_{HT} dependence of this high damage threshold transition, we postulate that a second mechanism to that described above is involved. For example, we note that T_{HT} ~1850 K corresponds to the softening point of fused silica where the viscosity is low enough to allow macroscopic, capillary-driven flow and healing of any residual micro- and nano-crack which limit the fracture toughness of the surface.

The present dicusssion suggests the use of laser annealed CVD as a means of mitigating optically damaged optical components for high power laser systems. To date all such laser based mitigation efforts have relied on the removal or reflow of material. In contrast the present mitigation approach would rely on an additive approach for the repair of damaged or defective material. To date few attempts have been made to replace material lost in the original damage event and thus restore the integrity of the wave propagating media. Indeed, laser-based chemical vapor deposition (L-CVD) is a proven technique for localizing material depositions in standard CVD vacuum chambers

which might be used to locally treat isolated damage sites [25]. Because of the high damage thresholds achieved, the present study on CVD deposited SiO_2 may provide a basis for the use of gas phase silica precursors in an L-CVD process as a means to locally deposit high damage threshold silica suitable for high power laser optics.

5. SUMMARY

A study was performed on high purity, defect rich SiO_2 films to probe the annealing behavior and role of the intrinsic defects as pertains to laser light absorption and damage. Defect populations were characterized using FTIR reflectivity, revealing non-bridging modes and a highly unrelaxed network of Si-O-Si bonds, while time-resolved broadband PL indicated highly interacting, optically-active defects with excited state lifetimes on the order of 3.2 ns. Rapid, localized CO_2 laser annealing at temperatures T_{HT} up to 2000 K enables bond reorganization, dehydroxylization and reduces PL from glass defects. While the transverse optic mode (TO_3) frequency monotonically shifted towards near pristine levels, both the broadband PL and non-bridging mode intensities from FTIR showed a slight increase near ~1600 K before decreasing at higher T_{HT}. The damage resistance of the annealed film was shown to increase with increasing T_{HT} and inverse scan rates to ~2x that of the underlying etched substrate. Our studies thus demonstrate that, regardless of the quality of CVD deposited silica, high temperature annealing can be performed to achieve substantially high damage threshold performance, allowing one to contemplate using CVD for damage repair of high energy laser optics.

ACKNOWLEDGEMENT

This work performed under the auspices of the U.S. Department of Energy by Lawrence Livermore National Laboratory under Contract DE-AC52-07NA27344.

REFERENCES

[1] N. Bloembergen, "Role of cracks, pores, and absorbing inclusions on laser-induced damage threshold at surfaces of transparent dielectrics," *Applied Optics*, vol. 12, pp. 661-664, 1973.

[2] T. A. Laurence, J. D. Bude, N. Shen, T. Feldman, P. E. Miller, W. A. Steele, *et al.*, "Metallic-like photoluminescence and absorption in fused silica surface flaws," *Applied Physics Letters*, vol. 94, Apr 13 2009.

[3] P. E. Miller, J. D. Bude, T. I. Suratwala, N. Shen, T. A. Laurence, W. A. Steele, *et al.*, "Fracture-induced subbandgap absorption as a precursor to optical damage on fused silica surfaces," *Optics Letters*, vol. 35, pp. 2702-2704, Aug 2010.

[4] R. N. Raman, M. J. Matthews, J. J. Adams, and S. G. Demos, "Monitoring annealing via CO_2 laser heating of defect populations on fused silica surfaces using photoluminescence microscopy," *Opt. Express*, vol. 18, pp. 15207-15215, 2010.

[5] L. Skuja, "The origin of the intrinsic 1.9 eV luminescence band in glassy SiO_2," *Journal of Non-Crystalline Solids*, vol. 179, pp. 51-69, Nov 1994.

[6] M. J. Matthews, C. W. Carr, H. A. Bechtel, and R. N. Raman, "Synchrotron radiation infrared microscopic study of non-bridging oxygen modes associated with laser-induced breakdown of fused silica," *Applied Physics Letters*, vol. 99, p. 151109, Oct 10 2011.

[7] J. Neauport, D. Valla, J. Duchesne, P. Bouchut, L. Lamaignere, J. Bigarre, *et al.*, "Building high damage threshold surfaces at 351 nm," *Optical Fabrication, Testing, and Metrology*, vol. 5252, pp. 131-139, 2004.

[8] R. M. Brusasco, B. M. Penetrante, J. A. Butler, S. M. Maricle, and J. E. Peterson, "CO_2 laser polishing for reduction of 351-nm surface damage initiation in fused silica," *Laser-Induced Damage in Optical Materials: 2001 Proceedings*, vol. 4679, pp. 34-39, 2002.

[9] P. A. Temple, W. H. Lowdermilk, and D. Milam, "Carbon-Dioxide Laser Polishing of Fused-Silica Surfaces for Increased Laser-Damage Resistance at 1064-Nm," *Applied Optics,* vol. 21, pp. 3249-3255, 1982.

[10] S. Papernov and A. W. Schmid, "Correlations between embedded single gold nanoparticles in SiO2 thin film and nanoscale crater formation induced by pulsed-laser radiation," *Journal of Applied Physics,* vol. 92, p. 5720, 2002.

[11] T. I. Suratwala, P. E. Miller, J. D. Bude, W. A. Steele, N. Shen, M. V. Monticelli, *et al.*, "HF-Based Etching Processes for Improving Laser Damage Resistance of Fused Silica Optical Surfaces," *Journal of the American Ceramic Society,* vol. 94, pp. 416-428, Feb 2011.

[12] S. T. Yang, M. J. Matthews, and S. Elhadj, "Thermal transport in CO_2 laser irradiated fused silica: in situ measurements and analysis " *Journal of Applied Physics,* 2009.

[13] J. Hue, P. Carrec, J. Dijon, and P. Lyan, "R-on-1 automatic mapping: a new tool for laser damage testing " presented at the Laser-Induced Damage in Optical Materials Boulder, CO, 1995.

[14] F. Iacona, G. Ceriola, and F. La Via, "Structural properties of SiO2 films prepared by plasma-enhanced chemical vapor deposition," *Materials Science in Semiconductor Processing,* vol. 4, pp. 43-46, Feb-Jun 2001.

[15] D. V. Tsu, G. Lucovsky, and B. N. Davidson, "Effects of the nearest neighbors and the alloy matrix on SiH stretching vibrations in the amorphous SiOr-H (0<r<2) alloy system," *Physical Review B,* vol. 40, pp. 1795-1805, Jul 1989.

[16] R. M. Almeida, T. A. Guiton, and C. G. Pantano, "Characterization of silica-gels by infrared reflection spectroscopy," *Journal of Non-Crystalline Solids,* vol. 121, pp. 193-197, May 1990.

[17] J. A. Theil, D. V. Tsu, and G. Lucovsky, "Reaction patheays and sources of OH groups in low-temperature remote PECVD silicon dioxide thin-films," *Journal of Electronic Materials,* vol. 19, pp. 209-217, Mar 1990.

[18] M. J. Matthews, R. M. Vignes, D. Cooke, S. T. Yang, and J. S. Stolken, "Analysis of microstructural relaxation phenomena in laser-modified fused silica using confocal Raman microscopy," *Optics Letters,* vol. 35, pp. 1311-1313, May 1 2010.

[19] C. T. Kirk, "Quantitative-Analysis of the Effect of Disorder-Induced Mode-Coupling on Infrared-Absorption in Silica," *Physical Review B,* vol. 38, pp. 1255-1273, Jul 15 1988.

[20] S. O. Kucheyev and S. G. Demos, "Optical defects produced in fused silica during laser-induced breakdown," *Applied Physics Letters,* vol. 82, pp. 3230-3232, May 12 2003.

[21] F. J. Himpsel, F. R. McFeely, A. Talebibrahimi, J. A. Yarmoff, and G. Hollinger, "Microscopic Structure Of The SiO_2/Si Interface," *Physical Review B,* vol. 38, pp. 6084-6096, Sep 1988.

[22] R. M. Almeida and C. G. Pantano, "Structural Investigation Of Silica-Gel Films By Infrared-Spectroscopy," *Journal of Applied Physics,* vol. 68, pp. 4225-4232, Oct 1990.

[23] M. J. Davis, "The effect of water on the viscosity of silicate melts: A configurational entropy approach," *Geochimica Et Cosmochimica Acta,* vol. 63, pp. 167-173, Jan 1999.

[24] M. von Allmen and A. Blatter, *Laser-Beam Interactions with Materials,* second ed. Hiedelberg: Springer-Verlag, 1998.

[25] J. Mazumder, P. S. Mohanty, and A. Kar, "Mathematical modelling of laser materials processing," *International Journal of Materials & Product Technology,* vol. 11, pp. 193-252, 1996.